Geosci. Instrum. Method. Data Syst. Discuss., 5, 247–283, 2015
www.geosci-instrum-method-data-syst-discuss.net/5/247/2015/
doi:10.5194/gid-5-247-2015

Geoscientific Instrumentation Methods and Data Systems Discussions
Open Access

Designing optimal greenhouse gas monitoring networks for Australia

T. Ziehn[1], R. M. Law[1], P. J. Rayner[2], and G. Roff[3]

[1]CSIRO Oceans and Atmosphere Flagship, Aspendale, VIC 3195, Australia
[2]School of Earth Sciences, University of Melbourne, Melbourne, VIC 3010, Australia
[3]Australian Bureau of Meteorology, Docklands, VIC 3008, Australia

Received: 30 June 2015 – Accepted: 19 July 2015 – Published: 5 August 2015

Correspondence to: T. Ziehn (tilo.ziehn@csiro.au)

Published by Copernicus Publications on behalf of the European Geosciences Union.

Abstract

Atmospheric transport inversion is commonly used to infer greenhouse gas (GHG) flux estimates from concentration measurements. The optimal location of ground based observing stations that supply these measurements can be determined by network design. Here, we use a Lagrangian particle dispersion model (LPDM) in reverse mode together with a Bayesian inverse modelling framework to derive optimal GHG observing networks for Australia. This extends the network design for carbon dioxide (CO_2) performed by Ziehn et al. (2014) to also minimize the uncertainty on the flux estimates for methane (CH_4) and nitrous oxide (N_2O), both individually and in a combined network using multiple objectives. Optimal networks are generated by adding up to 5 new stations to the base network, which is defined as two existing stations, Cape Grim and Gunn Point, in southern and northern Australia respectively. The individual networks for CO_2, CH_4 and N_2O and the combined observing network show large similarities because the flux uncertainties for each GHG are dominated by regions of biologically productive land. There is little penalty, in terms of flux uncertainty reduction, for the combined network compared to individually designed networks. The location of the stations in the combined network is sensitive to variations in the assumed data uncertainty across locations. A simple assessment of economic costs has been included in our network design approach, considering both establishment and maintenance costs. Our results suggest that while site logistics change the optimal network, there is only a small impact on the flux uncertainty reductions achieved with increasing network size.

1 Introduction

Carbon dioxide (CO_2), methane (CH_4) and nitrous oxide (N_2O) are the three most important greenhouse gases (GHGs) and they amount to 80 % of the total current radiative forcing from well mixed GHGs. Their concentrations in the atmosphere have increased since pre-industrial times by 40 % for CO_2, 150 % for CH_4 and 20 % for N_2O.

GID
5, 247–283, 2015

Their combined increases are the main driver for climate change (Ciais et al., 2013). It is therefore important to monitor major GHGs, not only for the continuous observation of atmospheric concentrations to detect global trends, but also for deriving better constrained budgets and a better attribution of the flux components.

Surface fluxes can be derived, for example, by running a process based model in forward mode, where atmospheric concentration measurements have been used to constrain model parameters. This has been successfully demonstrated for CO_2 in the form of the carbon cycle data assimilation system (CCDAS) (Rayner et al., 2005; Ziehn et al., 2011). However, the most commonly used tool for deriving surface fluxes on multiple temporal and spatial scales has been atmospheric transport inversion (e.g. Gurney et al., 2002; Peylin et al., 2013). Both approaches rely heavily on accurate measurements from observing stations.

A global network of ground based measurement stations has been developed over the years to monitor CO_2, CH_4 and N_2O. The Global Atmosphere Watch (GAW) programme of the World Meteorological Organization (WMO), for example, coordinates activities on greenhouse gas observations including quality assurance, calibration, validation, and archiving of data for climate research purposes. Stations are actively hosted by more than 80 countries around the world (WMO, 2014). Most of these stations perform flask sampling only (selected for background conditions) but continuous in-situ data are becoming increasingly available.

Network design studies can be used to provide guidance on how to extend existing observational networks in an optimal way, particularly as new types of instrument or measurements become available. One major advantage of network design is that stations can be assessed where no data are available yet and potential new stations can be added to the network by minimising a defined cost function. Most GHG network design studies have been performed for CO_2 only (e.g. Rayner et al., 1996; Law et al., 2004). However since current generation instruments now typically measure more than one GHG, and logistical benefits are derived from co-locating instruments, it is helpful to extend the CO_2 only studies to consider the network design requirements for the three major GHGs together.

We focus our study on the Australian continent and use the methodology developed by Ziehn et al. (2014), although the method could equally be applied to other regions (e.g. Nickless et al., 2015, for South Africa). We consider continuous concentrations measurements for all three GHGs at an hourly time scale which results in a network that could be used to derive surface fluxes at a high spatial and temporal resolution. Australia is an interesting case study since it is a large, mostly sparsely-populated, continent with only a small current GHG observing network compared to other continents such as North America and Europe. Haverd et al. (2013) noted that global inversions provided no meaningful constraint on the Australian carbon budget due to limited observations that were usually selected for background (i.e. ocean not continental) conditions. Hence, given resource constraints, it is vital that any additional measurement capability be targeted at locations with the greatest potential to reduce flux uncertainties across the three GHGs but also at locations that are logistically feasible and minimise ongoing maintenance costs. For this reason the network design process applied here is based on pre-selected potential locations, chosen for their existing infrastructure. We also test the sensitivity to a simple accessibility measure which would be a likely contributor to ongoing maintenance costs. Establishment and maintenance costs have also been considered in a network design study for a synthetic greenhouse gas in California (Lucas et al., 2014). While they did not pre-select locations, the establishment cost was chosen to be smaller for locations near to existing sites, while maintenance cost was related to measurement frequency (a factor that we do not consider to be relevant for our application).

2 Methodology

The approach used in this study for the network design is based on a combination of Bayesian inverse modelling methodology applied to an atmospheric transport model.

GID
5, 247–283, 2015

We only provide a short summary of the methodology here and refer for details to Ziehn et al. (2014).

A simple linear expression can be used to represent the relationship between surface fluxes ($\boldsymbol{f}$) and modelled concentrations ($\boldsymbol{c}_{\text{mod}}$)

$$\boldsymbol{c}_{\text{mod}} = \boldsymbol{c}_{\text{mod}_\text{f}} = \mathbf{T}\boldsymbol{f} \tag{1}$$

where $\mathbf{T}$ is the transport or sensitivity matrix which needs to be determined. If we omit contributions from outside the region of interest and the initial conditions, then our modelled concentrations are derived from surface fluxes only, i.e. $\boldsymbol{c}_{\text{mod}} = \boldsymbol{c}_{\text{mod}_\text{f}}$.

Using a Bayesian synthesis inversion scheme (Tarantola, 1987; Enting, 2002) and assuming a Gaussian error distribution for the surface fluxes and concentrations, we derive optimal surface fluxes $\boldsymbol{f}$ based on the observations provided and also posterior uncertainties for the GHG fluxes expressed through the posterior covariance matrix $\mathbf{C}_{\boldsymbol{f}}$. For the network design approach we are only interested in the latter, because our aim is to find a network (set of observations) that minimizes the surface flux uncertainties.

Incremental optimisation is then applied to design a network by adding one location at a time with each new location chosen to minimise a cost function. The cost function (Sect. 3.1) is calculated based on the posterior flux uncertainties.

As noted by Hardt and Scherbaum (1994), the calculation of the posterior flux uncertainties does not depend on a particular value of the surface fluxes or concentration observations. It only depends on the transport model, the prior flux uncertainties and observational uncertainties. We discuss each in turn.

2.1 Transport model

The relationship between surface fluxes and atmospheric concentrations is calculated using the Lagrangian Particle Dispersion Model (LPDM) (Uliasz, 1994) which we run in reverse mode for each potential and existing measurement station we would like to include in the network design process. Particles are released (from the known or proposed measurement height) every 20 s for a total of four weeks for all four seasons

GID
5, 247–283, 2015
Greenhouse gas network design
T. Ziehn et al.

of the year and the particle's position is recorded at 15 min intervals. Particles that are near the surface are counted for each grid cell to determine the surface influence or sensitivity, from which a source-receptor relationship can be defined (Seibert and Frank, 2004; Ziehn et al., 2014) as

$$\frac{\partial \overline{\chi}}{\partial \dot{q}_{\mathrm{in}}} = \frac{\Delta T g}{\Delta P} \overline{\left(\frac{N_{\mathrm{in}}}{N_{\mathrm{tot}}} \right)} \frac{M_{\mathrm{air}}}{M_x} \times 10^6, \tag{2}$$

where $\overline{\chi}$ is a volume mixing ratio (receptor) and $\dot{q}_{\mathrm{in}}$ is a mass flux density (source). N_{in} is the number of particles in a grid element (source) at each time interval ΔT and N_{tot} the total number of particles released during a time interval. The overbar indicates temporal averaging over the time interval ΔT. ΔP is the pressure difference in the surface layer and g is the gravity of Earth. M_{air} represents the molecular mass of air and M_x is the molecular mass of our quantity of interest, which is carbon C and nitrogen N, respectively. Other than the molecular mass scaling the source-receptor relationships are the same for all three greenhouse gases, on the assumption that any atmospheric loss of CH_4 or N_2O will have a negligible impact on the spatial pattern of surface influence over the relatively short periods being modelled.

LPDM requires meteorological driving fields which are provided in this study by the regional version of the Australian Community Climate and Earth System Simulator (ACCESS-R) (NMOC, 2013) at 12 km resolution for the Australian region at an hourly time scale. Driving data include the 3-D wind field, temperature and turbulent kinetic energy (TKE) at 39 vertical levels up to 18 km in height. Ziehn et al. (2014) only calculated source-receptor relationships for one summer and one winter month. Here, we also run LPDM for the intermediate seasons, and calculate source-receptor relationships for January, April, July and October.

Since LPDM is run over a limited area, any boundary effects need to be assessed. This was done by Ziehn et al. (2014) who found that the uncertainty contribution of the boundary concentrations to the uncertainy of the observations could be considered

GID
5, 247–283, 2015

negligible. This finding is equally applicable to CH_4 and N_2O as CO_2 and hence we do not include boundary concentrations in the network design process.

2.2 Prior flux uncertainties

The Bayesian inversion method requires an estimate of the prior surface flux uncertainties, which are incorporated in the error covariance matrix for prior surface fluxes. Here, we do not consider correlations between different fluxes which means the error covariance matrix only has elements in the diagonal. The effect of temporal correlations for the same grid cell and spatial correlations for neighbouring grid cells for surface fluxes was investigated by Nickless et al. (2015) and they found that the correlation structure has a significant impact on the results of the network design. However, in order to include correlations in the prior error covariance matrix one needs to be confident in the size and structure of those correlations (Rayner, 2004). Including, for example, correlations that are too large can lead to an over constrained system (Lauvaux et al., 2012; Nickless et al., 2015). We therefore decided to assume independence between prior fluxes.

The prior flux uncertainties are provided at a weekly temporal resolution and separately for daytime and nighttime, consistent with the weekly temporal resolution at which fluxes are estimated. Flux uncertainties are expressed as one standard deviation.

2.2.1 CO_2 prior flux uncertainties

The CO_2 prior flux uncertainties are calculated in the same manner as Ziehn et al. (2014), combining contributions from the terrestrial biosphere (Fig. 1) and fossil fuel combustion. The additional two seasons, not used in Ziehn et al. (2014), have larger prior uncertainty contributions from the terrestrial biosphere, with maximum values in Queensland in April and in south eastern Australia in October. As well as varying by season, CO_2 prior flux uncertainties vary by week within the season, but the same prior uncertainties are used for day and night.

GID
5, 247–283, 2015

Greenhouse gas network design

T. Ziehn et al.

2.2.2 CH_4 prior flux uncertainties

Prior CH_4 flux uncertainties are assumed to be proportional to estimated CH_4 fluxes. Total CH_4 emissions are taken from the Australian CH_4 budget of Fraser et al. (2011). Here, we consider contributions from anthropogenic sources such as ruminant animals, coal mining, oil production and landfills as well as contributions from natural sources including wetlands, termites and coastal ocean. For each sector (except coastal ocean which we take as uniform), we generate a simple spatial distribution of fluxes (at the network design resolution) assuming three different flux levels (high, moderate and low) which we scale to the sector total. Although, this provides only a crude approximation of the real flux distribution it is sufficient in this case due to the large uncertainties that we assign to the fluxes (50 % of their value). Emissions from wetlands vary seasonally whereas emissions from other sectors are assumed to be constant throughout the year. Derived prior flux uncertainties for ruminant animals and the Australian total are presented in Fig. 2. All variances are multiplied by the land fraction in a similar way to CO_2 (Ziehn et al., 2014); however variances for coastal ocean fluxes are multiplied with the ocean fractions instead and variances for fluxes from oil production are not multiplied by land or ocean fractions because we consider contributions from both, offshore and onshore.

The largest anthropogenic source of CH_4 in Australia is due to enteric fermentation from ruminant animals accounting for about 2.1 $TgC\,yr^{-1}$. Here we include emissions from the dairy and beef industry and from sheep grazing (ABS, 2005; MLA, 2011a, b). Fluxes are assigned based on the distribution and density of animals with the largest concentration to be found in New South Wales (NSW), Queensland (QLD) and Victoria (VIC). Coal mining accounts for about 0.6 $TgC\,yr^{-1}$ with the largest density of coal mines found in NSW and QLD (GA, 2012). Emissions from oil production sum up to about 0.5 $TgC\,yr^{-1}$. The majority of the oil basins are located offshore along the coast of Western Australia (WA) and VIC (GA, 2010). Landfills also contribute by about

GID
5, 247–283, 2015

0.5 $TgC\,yr^{-1}$ and are spread out across the continent with the highest concentration near populated areas (DOE, 2013).

Wetlands are one of the largest natural sources of CH_4 in Australia with a flux of about 1.1 $TgC\,yr^{-1}$. Emissions depend mainly on temperature and ground water (Bloom et al., 2010) and the tropical north of Australia shows a strong seasonality with highest emissions during the wet season and soon after (December–May) (Fraser et al., 2011). Wetlands in the south of Australia show a peak in emissions during spring time (October–November) with a minimum during late autumn and winter (Bloom et al., 2012; Loh et al., 2015). The spatial distribution of the wetland CH_4 fluxes used in this study is based on Australian annual mean rainfall with a seasonality as described above. Emissions from coastal oceans surrounding Australia are estimated to be about 1.1 $TgC\,yr^{-1}$. Termites contribute about 1.0 $TgC\,yr^{-1}$ and are present throughout Australia. The largest contribution however comes from the tropical north. Emissions from termites are not well characterized which results in large uncertainties (Fraser et al., 2011).

2.2.3 N_2O prior flux uncertainties

We derive prior uncertainties for N_2O fluxes based on emissions from agriculture. In Australia, almost 80 % of N_2O is emitted from agricultural land accounting for about 60 $ktN\,yr^{-1}$ (Dalal et al., 2003). The total annual flux is distributed across Australia at the network design resolution using three different levels (as for CH_4) based on Australia's land uses (DOA, 2006). We assign larger fluxes to irrigated areas, because N_2O emissions are generally higher from poorly drained soils and irrigation tends to increase the chance of the soils becoming waterlogged (Dalal et al., 2003). Finally, we assign the prior flux uncertainties of N_2O to be 50 % of the flux value as shown in Fig. 3a.

GID
5, 247–283, 2015
Greenhouse gas network design
T. Ziehn et al.

2.3 Observational uncertainties

Observational uncertainties include measurement, transport and aggregation errors and if not stated otherwise we assume the same uncertainties for all existing and potential measurement stations. In the standard case, we set the observational uncertainties to 2 ppm for CO_2, to 4 ppb for CH_4 and 0.1 ppb for N_2O.

3 Set up and data

The network design for Australia is performed on a $1.8^\circ \times 1.8^\circ$ grid resolution by running LPDM in backward mode for stations that we would like to include in this study. Each station is assessed in terms of its ability to reduce the uncertainty on CO_2, CH_4 and N_2O flux estimates. Incremental optimisation is used to find the station for which our cost function (Sect. 3.1) is minimal. This station is then removed from the candidate list (Sect. 3.2) and we repeat the incremental optimization until the final size of the new network is reached. In this study we add a maximum of 5 new stations to the base network.

3.1 Cost function for network design

The aim of the network design is to reduce the uncertainties on GHG flux estimates by minimising a cost function. In order to do this we require a scalar quantity which we obtain from the posterior covariance matrix by summing over all elements (uncertainty of the integrated flux). The cost function J is then defined as:

$$J = \sqrt{\sum_{i=1}^{n} \sum_{j=1}^{n} C_{f_{ij}}} \tag{3}$$

where n is the number of elements in the diagonal of the matrix $\mathbf{C}_f$.

GID
5, 247–283, 2015
Greenhouse gas network design
T. Ziehn et al.

We apply incremental optimisation to minimise J and design observational networks for each of the 3 GHGs individually. The design of an optimal network which considers all 3 GHGs together at the same time requires a multi-objective optimization approach. The simplest way of solving a multi-objective problem is to combine its multiple objectives into a single objective scalar function which is also know as a weighted sum. The advantage of this approach is that we can still use the incremental optimisation method. However, a significant drawback is that we need to choose appropriate weights for each of the objectives which can be challenging.

The new cost function J_m that combines multi-objectives is defined as:

$$J_m = \sqrt{\left(J_{CO_2} w_{CO_2}\right)^2 + \left(J_{CH_4} w_{CH_4}\right)^2 + \left(J_{N_2O} w_{N_2O}\right)^2} \quad (4)$$

where J_{CO_2}, J_{CH_4} and J_{N_2O} are the objective cost functions for the 3 GHGs, CO_2, CH_4 and N_2O respectively. We use the global-warming potential (GWP) for a 100 years time horizon as the weight for each GHG, i.e. $w_{CO_2} = 1$, $w_{CH_4} = 34$ and $w_{N_2O} = 298$ (Myhre et al., 2013).

Each network is evaluated in terms of the uncertainty reduction U_R we achieve, with U_R defined as:

$$U_R = 1 - \frac{\hat{J}}{J^*} * 100\,\% \quad (5)$$

where $\hat{J}$ is the optimal cost function value and J^* is the cost function values based on the prior uncertainties.

3.2 Existing network and potential stations

Although Australia already commands a network of 9 ground based measurement stations as listed in Table 1 with their locations shown in Fig. 4a, only 6 of them are currently operational. For the base network we further select 2 of those 6 stations, located

GID
5, 247–283, 2015

at Cape Grim and Gunn Point, for the following reasons: (1) both stations are part of the WMO/GAW global monitoring network and the Southeast Asia-Australian regional network. (2) Both stations are managed by the Australian Bureau of Meteorology (BoM) with the Commonwealth Scientific and Industrial Research Organisation (CSIRO) providing GHG research strategy. (3) Both stations provide in situ measurements for CO_2, CH_4 and N_2O.

For the network design, we introduce a scaling factor a_{obs} in order to distinguish between the difference in quality of observations we expect to obtain from different sites. For example, for Cape Grim we set a_{obs} to 0.5, which means that we halve the observational uncertainties for CO_2, CH_4 and N_2O in comparison to what we assume in the standard case (see Sect. 2.3). Similar, for Gunn Point we choose $a_{obs} = 0.75$ to reflect the high accuracy of observation we expect from this station. For all other existing stations a_{obs} is set to 1.

There are many ways of setting up a list of potential stations that one would like to include in the network design process. Commonly those stations are assigned according to a regular grid that covers the whole modelling domain. Depending on the resolution chosen, one might end up with a large list of stations that need to be assessed. Many of these potential stations might be located in inaccessible areas where it would be impossible to set up and maintain a new measurement site. Therefore, it is more beneficial to pre-select potential station locations according to a certain criteria, for example, by making use of existing infrastructure.

Here, we use mainly the locations of the Australian BoM weather watch radar stations (NRL, 2014) as potential stations. This guarantees that all stations are accessible by road, have power available and are maintained. The list of all 59 BoM stations can be found in Table 2 with their location shown in Fig. 4b. We also include one additional potential station, the Lucinda Jetty Coastal Observatory, which is currently used to collect optical data on the coastal waters and the atmosphere.

3.3 Sensitivity tests

The sensitivity of the network design to certain parameters used to obtain the source-receptor relationship and choices in the set-up of the network design and their consequences on the results has already been investigated by Nickless et al. (2015). Here, we focus on 5 different sensitivity tests, which are related to the weights assigned in the cost function for the multi-objective optimization and the importance of prior flux uncertainties and observational uncertainties on the outcome of the network design.

SE1 In the first sensitivity test we choose the weights in the cost function J_m such that each single objective contributes equally to the multi-objective problem, i.e. by normalizing with the prior cost function values J^* using $w_{CO_2} = 1/J^*_{CO_2}$, $w_{CH_4} = 1/J^*_{CH_4}$ and $w_{N_2O} = 1/J^*_{N_2O}$. In this way we ensure that no priority is given to a GHG with larger prior flux uncertainty values.

SE2 The second sensitivity test focuses on the way we assign observational uncertainties for stations not in the base network. Rather than use the same uncertainty for all potential stations, we double the uncertainty for sites close to large GHG sources ($a_{obs} = 2$). The assumption is that sites close to large sources will have "noisier" measurements and may be more difficult to model and this should be accounted for by a larger observational uncertainty.

We test the impact of the increased uncertainties on the network design. The scaling factor a_{obs} that we use for this sensitivity test is provided in Tables 1 and 2 for each of the stations and GHGs investigated here.

SE3 In a third sensitivity experiment we look at the impact of the way we derive the prior flux uncertainties for CH_4 and N_2O. In contrast to the prior flux uncertainties for CO_2 which are derived from high resolution model simulations with daily output, the prior flux uncertainties for CH_4 and N_2O are based an annual budgets with a spatial distribution generated using density maps from various sectors as

GID
5, 247–283, 2015

described in Sect. 2.2. We acknowledge that the spatial pattern and the magnitude of the flux components we derive in this way are to some degree arbitrary. In order to test the impact of our prior flux uncertainties for CH_4 and N_2O on the network design results we randomly vary assigned fluxes for each sector in the following way: (a) if a grid cell already has a flux assigned we randomly vary the current flux by a maximum of ±25 % and (b) if a grid cell has a zero flux we give that grid cell a 50 % chance of a flux at a moderate level. Flux uncertainties are then derived as before by using 50 % of the assigned flux value.

SE4 Although, the focus of this study is not on minimising exact economic costs associated with setting up and maintaining a new station, in the fourth sensitivity experiment we include the distance d from Aspendale (as the location of the base laboratory from which a network could be run) to any other existing or potential station by adding the following term to the cost function:

$$J_{\mathrm{md}} = J_m + \frac{d}{\max(d)} w_d . \tag{6}$$

The distance to a remote site is a possible factor in the maintenance costs for a site, assuming service visits require staff to travel from the base laboratory. We also introduce a weight factor w_d to scale the overall importance of the distance in the cost function.

SE5 In a final sensitivity test we combine SE2 and SE4 to consider increased observational uncertainties together with distance for the combined optimisation using GWP weights in the cost function.

GID
5, 247–283, 2015

4 Results and discussion

4.1 Base network

Our base network consists of only 2 stations, Cape Grim and Gunn Point. However, observations from those two stations are already able to significantly reduce the uncertainties on GHG flux estimates for Australia as shown in Table 3. Gunn Point is the most important station in terms of its ability to reduce uncertainties on CO_2 flux estimates (about 11 %), whereas Cape Grim is the most important station in terms of its ability to reduce uncertainties on CH_4 and N_2O flux estimates (about 8 and 10 %, respectively). Overall, both stations together are able to reduce the uncertainties on all 3 GHG flux estimates between 12 and 17 %.

4.2 Extended networks

We first design optimal network extensions for each GHG individually by adding up to 5 new stations to the base network using incremental optimization as described earlier. The ranking of the new stations is presented in Table 4 with their uncertainty reduction show in Fig. 5a and their location shown in Fig. 6a.

The CO_2 network extension is similar to the one derived in Ziehn et al. (2014), despite using a different base network (2 instead of 6 stations) and using all 4 seasons (instead of only 2 seasons) as driving data. The first station that is added to the base network is located at Charleville, which is the only station that was not included in the network derived in Ziehn et al. (2014). This is mainly driven by the large prior biosphere flux uncertainties in April in the eastern part of the Australian continent (see Fig. 1b). The other 4 stations added to the network are identical to the ones selected in Ziehn et al. (2014). The new optimal CO_2 observing network is able to reduce the CO_2 flux uncertainties by about 47 % and consists of 3 stations in the tropical north (Gunn Point, Wyndham and Mornington Island), 2 stations in eastern Australia (Charleville and Moree) and 2 stations in the south east of Australia (Cape Grim and Tumbarumba).

GID
5, 247–283, 2015

The network extension focussing on CH_4 only is similar to the optimal CO_2 network extension due to a similar distribution of prior flux uncertainties at least for the eastern part of the Australian continent. Tumbarumba becomes the most important station in the CH_4 network extension and, as in the CO_2 case, Moree is the second most important location. However, the optimization also places a station in Perth on the west coast of Australia, which was not required for CO_2. In total we are able to achieve a reduction of about 32 % on CH_4 flux uncertainties.

The optimal N_2O network shows some similarities with the optimal CO_2 and CH_4 network. Moree is added first by the optimization, which highlights the importance of this location for all 3 GHGs. Three stations in the N_2O observing network are located in the south east (Cape Grim, Broadmeadows and Captains Flat), which is the region where we also assume the largest prior flux uncertainties. The new N_2O network is able to reduce the N_2O flux uncertainties by about 38 %.

We now use the cost function that combines multi-objectives (Eq. 4) to design a network that is optimal for all 3 GHGs combined. Although, the ranking of the stations shown in Table 4 is for the combined network, the uncertainty reduction is calculated for each GHG individually (Fig. 5b) to make it comparable with the previous networks. From the ranking of the stations in Table 4 we can see that the optimal combined network is exactly the same as the optimal CO_2 only network. This is due to the way the weights are assigned for the contributions of all 3 GHGs (according to the GWP); priority is given to the reduction of CO_2 flux uncertainties, because the prior CO_2 fluxes have by far the largest uncertainties.

Given that the optimal combined network is the same as the optimal CO_2 network the reduction in uncertainty for CO_2 is unchanged. For CH_4 and N_2O uncertainty reductions are 30 and 33 %, only 2 and 5 % less than for the individual networks.

4.3 Sensitivity tests

Sensitivity test SE1 changes the weights in the cost function J_m so that each single objective for the 3 GHGs contributes equally to J_m (Sect. 3.3) despite the order of magnitude difference in the prior flux uncertainty values for each of the 3 GHGs (Figs. 1 to 3). Table 5 and Fig. 6b indicate that the network based on equal weights is somewhat different to the network based on GWP weights. Moree, Tumbarumba and Mornington Island appear in both networks, but the network based on equal contributions now includes Perth (instead of Wyndham) and Longreach (instead of Charleville,) which are stations that were only included in the CH_4 and N_2O networks (Table 4). In particular, a station in Perth does not significantly contribute to a reduction in CO_2 flux uncertainties, but is selected now that a reduction of flux uncertainties is equally important for all 3 GHGs. The replacement of Charleville with Longreach is only a minor change since both stations are located in roughly the same region in the east of the continent.

As expected the SE1 network trades off decreased uncertainty reductions for CO_2 with increased uncertainty reductions for CH_4 and N_2O (Fig. 5b). However the changes in uncertainty reduction are relatively small, at only 2–4 % for the networks with five additional sites.

Networks for the SE2 test were optimised for each GHG individually using increased observational uncertainties for sites that are expected to be close to large fluxes. For CO_2 the new network (Fig. 6c) is mostly different from the previous one since the original network contained three sites (Charleville, Moree, Tumbarumba) that we penalised for being close to large sources. All are removed from the new network, being replaced by Marburg, Captains Flat and Coffs Harbour which are closer to the east coast. Interestingly the optimisation also chose to replace Wyndham with Tennant Creek despite Wyndham not having an increased observational uncertainty. However, in this configuration both stations provide about the same reduction in uncertainty and are therefore interchangeable. The uncertainty reduction for the SE2 CO_2 network was 4 % lower than for the original network (Fig. 5c).

For CH_4, only one site (Perth) in the standard network was allocated an increased uncertainty and the SE2 optimisation produces the same network, retaining Perth though adding it to the network as additional site 4 rather than site 3 in terms of the ranking. The increased observational uncertainty for Perth results in a slightly smaller flux un-

GID
5, 247–283, 2015

certainty reduction. We also explored replacing Perth with either Geraldton or Albany which do not have increased observational uncertainties for SE2 and this would result in a network with almost the same performance.

Large N_2O sources are mainly located in the south-east of the country and two stations (Captains Flat and Broadmeadows) from the previous optimal N_2O network are allocated higher observational uncertainty in SE2. Consequently these are dropped from the new optimal N_2O network, being replaced by different locations in SE Australia (Tumbarumba and Mildura). The performance of the new network is comparable to the standard case.

SE3 assessed the impact of changing the prior CH_4 and N_2O flux values and their distribution, finding only a minor impact on the optimal CH_4 and N_2O network. For CH_4, Moree, Perth and Longreach remain in the optimal network. Tumbarumba in the south-east is replaced by Captains Flat also in the south-east and Wyndham located in the north is replaced by Halls Creek also located in the north, but further inland. For N_2O the change in flux uncertainties produces a different ranking of sites but only one change in selected sites; Broadmeadows in the south is replaced by Charleville in the east of the country. At first it seems surprising that Broadmeadows is dropped from the network taking into account the large N_2O uncertainties in Victoria. However, Cape Grim in the base network already constrains fluxes from Victoria and the random change in prior N_2O fluxes has also led to a reduction in the prior uncertainties for south east Australia.

Sensitivity tests SE4 (standard observational uncertainties) and SE5 (observational uncertainties from SE2) included the distance of stations to Aspendale as an additional criteria in the cost function used for determining a combined network (with GWP weights for the 3 different GHGs). The sum of distances to the 5 stations in the original network is about 8200 km. If we add the distance to the cost function setting $w_d = 10$ we obtain network extensions (Table 5, Figs. 5d and 6d) for both SE4 and SE5 where the sum of station distances is reduced to about 4000 km. For SE4 the new network retains Moree and Tumbarumba, and adds Longreach and Williamtown to the network in the east of the country. The final station in the SE4 optimal network extension is Broadmeadows, which is very close to Aspendale (base laboratory). For SE5 two locations (Longreach and Moree) are the same as for SE4; the other three sites are relatively close to those selected for SE4 but are chosen in preference to the SE4 selection because their CO_2 observational uncertainty is lower.

The additional distance constraint in our multi-objective problem means that we generally see a decrease in the performance of the new networks. Compared to the standard combined network, the reduction in flux uncertainty for SE4 is lower by about 4.5 % for CO_2 and 1 % for CH_4 but larger for N_2O by 3.5 % (Fig. 5). This is because the largest prior flux uncertainties for N_2O are located in the south-east of the country and hence N_2O benefits from moving the network closer to Aspendale in SE Australia. For SE5, the flux uncertainty is further decreased for CO_2 and CH_4 (8.5 and 2.5 %), but still slightly larger for N_2O by 1 % if compared to the standard combined network.

We also varied the weights w_d in SE4 to assess the performance of the optimal network with respect to the sum of stations distances as show in Fig. 7a. For CO_2 and CH_4 the performance of the network decreases relativiely slowly when decreasing the stations total distance from about 8200 km to about 3000 km (6 % decrease for CO_2 and 3 % decrease for N_2O), but drops significantly for CO_2 after that. The network performance for N_2O is increasing by about 3 % for the reasons given above before it drops at about 4000 km.

4.4 Limitations

When we add more constraints to the cost function or increase the observational uncertainties for our stations then we expect that the performance of the optimal network expressed through the uncertainty reduction will be reduced. Although, this is generally true for the full network extension consisting of 5 additional stations, we notice that, for example, by adding only two stations the performance of the CO_2 only network is actually slightly worse than the performance of the combined network using equal contributions of the 3 GHG in the cost function (Fig. 5a, b). This is because the incremental optimisation adds one station at a time, which maximizes the performance of the network only at each stage. The incremental optimisation is not able to assess benefits that may arise by adding a number of stations at the same time which other optimization methods such as the genetic algorithm (Rayner, 2004; Lucas et al., 2014) are able to do. However, Nickless et al. (2015) found that the genetic algorithm provided only marginally better solutions if compared with the incremental optimisation, but at a much larger computational cost.

Due to the fact that we pre-select the location of new stations through a list of potential sites we impose an initial constraint on the network design. Even if we include all potential stations in our network we would only achieve an uncertainty reduction of about 70 % for CO_2 in the standard case (Fig. 7b). Lowering the observational uncertainty to almost zero for all stations only provides an additional 5 % in uncertainty reduction for all stations to the network. This indicates that our network design is ultimately limited by our pre-selection of sites rather than our ability to model the GHG concentrations at those sites. Given that almost all of our optimal networks selected inland sites in eastern Australia ahead of coastal sites, this study would suggest that additional locations with existing infrastructure should be identified in inland NSW and Queensland to supplement our potential site list which, using the BoM radar network, is biased to coastal or near-coastal locations.

5 Summary and conclusions

In this study we used the Bayesian framework and a Lagrangian particle dispersion model in reverse mode to design optimal GHG observing networks for Australia individually for the 3 GHGs and together through a combination of multi-objectives with weights assigned to each GHG. The choice of weights would depend on the network design application. Only when we chose the weights in a way that ensured that each single objective contributed equally to the multi-objective problem were we able to de-

GID
5, 247–283, 2015

rive an optimal combined network that did not favour one of the 3 GHGs; a GWP-based weighting clearly favoured CO_2.

Due to similarities in the distribution of the prior flux uncertainties for the 3 GHGs, we obtained optimal individual and combined networks that showed a number of similarities, which is a positive outcome for any application of this study to investment in new sites. Most stations in the network extensions are located in the eastern part of the Australian continent (e.g. Moree and Tumbarumba) with a few stations in the north. For CH_4 and N_2O, a site in SW Australia is also of value.

The assignment of appropriate observational uncertainties to each station was found to be critical; network selection avoided sites that were assigned a larger uncertainty, replacing them with sites further from large sources and resulting in a small penalty in the overall effectiveness of the network for reducing flux uncertainty. Future work should be directed to better characterising the observational uncertainty for different sites, particularly at the component that accounts for our ability (or inability) to model GHG concentrations at specific locations. Observations from our existing network could be used for this characterisation as they span a range of site conditions. For example, Tumbarumba, which is often selected by the network design, is a forested site which may be challenging to model. Though not currently operational, existing measurements could be used to test assumptions about observational uncertainties.

Economic costs were included in two ways. Firstly, we pre-selected potential stations to account for existing infrastructure. In fact, we only included potential stations that were already set-up and maintained for other measurement purposes. This places an initial constraint on the network design which means that even with almost no observational error we would only achieve a uncertainty reduction of 75 % for CO_2 with all potential stations included in our network. Secondly, we included the distance from Aspendale (location of the base laboratory) to all other stations as a measure of maintenance costs in the cost function. We demonstrated that the total distance to the additional 5 stations in the optimal combined network can be more than halved with only a slight decrease in the performance of the network. By changing the weights for the

GID
5, 247–283, 2015

distance the user can decide if the priority is on a more cost efficient network or a network that provides the largest overall reduction in GHG flux uncertainties.

We conclude, that an optimal measurement network designed for CO_2 only also performs well for CH_4 and N_2O. This is due to large similarities in the pattern of the prior flux uncertainties derived for each of the 3 GHGs. This might change if we are able to obtain more detailed information particularly on the CH_4 and N_2O flux distribution and increase the resolution so that point sources (i.e. fossil fuel emissions) become more important.

Acknowledgements. Peter Rayner is in receipt of an Australian Professorial Fellowship (DP1096309).

References

ABS: Australia's beef cattle industry, Australian Bureau of Statistics, available at: http://www.abs.gov.au/ausstats/abs@.nsf/Previousproducts/1301.0Feature%20Article232005?opendocument (last access: 26 May 2015), 2005. 254

Bloom, A. A., Palmer, P. I., Fraser, A., Reay, D. S., and Frankenberg, C.: Large-scale controls of methanogenesis inferred from methane and gravity spaceborne data, Science, 327, 322–325, doi:10.1126/science.1175176, 2010. 255

Bloom, A. A., Palmer, P. I., Fraser, A., and Reay, D. S.: Seasonal variability of tropical wetland CH_4 emissions: the role of the methanogen-available carbon pool, Biogeosciences, 9, 2821–2830, doi:10.5194/bg-9-2821-2012, 2012. 255

Ciais, P., Sabine, C., Bala, G., Bopp, L., Brovkin, V., Canadell, J., Chhabra, A., DeFries, R., Galloway, J., Heimann, M., Jones, C., Le Quèrè, C., Myneni, R., Piao, S., and Thornton, P.: Carbon and Other Biogeochemical Cycles, book section 6, 465–570, Cambridge University Press, Cambridge, UK and New York, NY, USA, doi:10.1017/CBO9781107415324.015, 2013. 249

Dalal, R. C., Wang, W., Robertson, G. P., and Parton, W. J.: Nitrous oxide emission from Australian agricultural lands and mitigation options: a review, Austral. J. Soil Res., 41, 165–195, doi:10.1071/SR02064, 2003. 255

GID

5, 247–283, 2015

DOA: Land use in Australia, Department of Agriculture, available at: http://www.agriculture.gov.au/abares/aclump/Documents/Land_use_in_Australia_at_a_glance_2006.pdf (last access: 26 May 2015), 2006. 255

DOE: National Waste Reporting, Department of the Environment, available at: http://www.environment.gov.au/system/files/resources/0a517ed7-74cb-418b-9319-7624491e4921/files/overview-infrastructure_0.pdf (last access: 26 May 2015), 2013. 255

Enting, I. G.: Inverse Problems in Atmospheric Constituent Transport, Cambridge Univ. Press, New York, 2002. 251

Fraser, A., Chan Miller, C., Palmer, P. I., Deutscher, N. M., Jones, N. B., and Griffith, D. W. T.: The Australian methane budget: Interpreting surface and train-borne measurements using a chemistry transport model, J. Geophys. Res.-Atmos., 116, D20306, doi:10.1029/2011JD015964, 2011. 254, 255

GA: Australian oil resources, Geoscience Australia, available at: http://www.ga.gov.au/scientific-topics/energy/resources/petroleum-resources/oil (last access: 26 May 2015), 2010. 254

GA: Australian in situ coal resources, Geoscience Australia, available at: http://www.ga.gov.au/corporate_data/74097/74097.pdf (last access: 26 May 2015), 2012. 254

Gurney, K. R., Law, R. M., Denning, A. S., Rayner, P. J., Baker, D., Bousquet, P., Bruhwiler, L., Chen, Y., Ciais, P., Fan, S., Fung, I. Y., Gloor, M., Heimann, M., Higuchi, K., John, J., Maki, T., Maksyutov, S., Masarie, K., Peylin, P., Prather, M., Pak, B. C., Randerson, J., Sarmiento, J., Taguchi, S., Takahashi, T., and Yuen, C.: Towards robust regional estimates of CO_2 sources and sinks using atmospheric transport models, Nature, 405, 626–630, doi:10.1038/415626a, 2002. 249

Hardt, M. and Scherbaum, F.: The design of optimum networks for aftershock recordings, Geophys. J. Int., 117, 716–726, doi:10.1111/j.1365-246X.1994.tb02464.x, 1994. 251

Haverd, V., Raupach, M. R., Briggs, P. R., J. G. Canadell., Davis, S. J., Law, R. M., Meyer, C. P., Peters, G. P., Pickett-Heaps, C., and Sherman, B.: The Australian terrestrial carbon budget, Biogeosciences, 10, 851–869, doi:10.5194/bg-10-851-2013, 2013. 250

Lauvaux, T., Schuh, A. E., Uliasz, M., Richardson, S., Miles, N., Andrews, A. E., Sweeney, C., Diaz, L. I., Martins, D., Shepson, P. B., and Davis, K. J.: Constraining the CO_2 budget of the corn belt: exploring uncertainties from the assumptions in a mesoscale inverse system, Atmos. Chem. Phys., 12, 337–354, doi:10.5194/acp-12-337-2012, 2012. 253

Law, R. M., Rayner, P. J., and Wang, Y. P.: Inversion of diurnally varying synthetic CO_2: Network optimization for an Australian test case, Global Biogeochem. Cy., 18, GB1044, doi:10.1029/2003GB002136, 2004. 249

Loh, Z. M., Law, R. M., Haynes, K. D., Krummel, P. B., Steele, L. P., Fraser, P. J., Chambers, S. D., and Williams, A. G.: Simulations of atmospheric methane for Cape Grim, Tasmania, to constrain southeastern Australian methane emissions, Atmos. Chem. Phys., 15, 305–317, doi:10.5194/acp-15-305-2015, 2015. 255

Lucas, D. D., Yver Kwok, C., Cameron-Smith, P., Graven, H., Bergmann, D., Guilderson, T. P., Weiss, R., and Keeling, R.: Designing optimal greenhouse gas observing networks that consider performance and cost, Geosci. Instrum. Method. Data Syst., 4, 121–137, doi:10.5194/gi-4-121-2015, 2015. 250, 266

MLA: Australia's beef industry, Meet & Livestock Australia, available at: http://www.mla.com.au/files/d0faf79a-7218-4f5a-85db-a1110102aaf8/Cattle-Numbers-Map_as-at-June-2011.pdf (last access: 26 May 2015), 2011a. 254

MLA: Australia's sheepmeat industry, Meet & Livestock Australia, available at: http://www.mla.com.au/files/15f9de69-f6ec-44c3-87b5-a1110102e972/Sheep-Numbers-Map_as-at-June-2011.pdf (last access: 26 May 2015), 2011b. 254

Myhre, G., Shindell, D., Breon, F.-M., Collins, W., Fuglestvedt, J., Huang, J., Koch, D., Lamarque, J.-F., Lee, D., Mendoza, B., Nakajima, T., Robock, A., Stephens, G., Takemura, T., and Zhang, H.: Anthropogenic and Natural Radiative Forcing, book section 8, Cambridge University Press, Cambridge, UK and New York, NY, USA, 659–740, doi:10.1017/CBO9781107415324.018, 2013. 257

Nickless, A., Ziehn, T., Rayner, P. J., Scholes, R. J., and Engelbrecht, F.: Greenhouse gas network design using backward Lagrangian particle dispersion modelling – Part 2: Sensitivity analyses and South African test case, Atmos. Chem. Phys., 15, 2051–2069, doi:10.5194/acp-15-2051-2015, 2015. 250, 253, 259, 266

NMOC: APS1 upgrade of the ACCESS-R Numerical Weather Prediction system, Tech. Rep. Operations Bulletin Number 98, National Meteorological and Oceanographic Centre, available at: http://www.bom.gov.au/australia/charts/bulletins/apob98.pdf (last access: 5 August 2015), 2013. 252

NRL: Bureau of Meteorology National Radar Loop: Weather Watch Radars, Bureau of Meteorology, available at: http://www.bom.gov.au/australia/radar/ (last access: 26 May 2015), 2014. 258

Peylin, P., Law, R. M., Gurney, K. R., Chevallier, F., Jacobson, A. R., Maki, T., Niwa, Y., Patra, P. K., Peters, W., Rayner, P. J., Rödenbeck, C., van der Laan-Luijkx, I. T., and Zhang, X.: Global atmospheric carbon budget: results from an ensemble of atmospheric CO_2 inversions, Biogeosciences, 10, 6699–6720, doi:10.5194/bg-10-6699-2013, 2013. 249

Rayner, P. J., Enting, I. G., and Trudinger, C. M.: Optimizing the CO_2 observing network for constraining sources and sinks, Tellus B, 48, 433–444, doi:10.1034/j.1600-0889.1996.t01-3-00003.x, 1996. 249

Rayner, P. J., Scholze, M., Knorr, W., Kaminski, T., Giering, R., and Widmann, H.: Two decades of terrestrial carbon fluxes from a carbon cycle data assimilation system (CCDAS), Global Biogeochem. Cy., 19, GB2026, doi:10.1029/2004GB002254, 2005. 249

Rayner, R. J: Optimizing CO_2 observing networks in the presence of model error: results from TransCom 3, Atmos. Chem. Phys., 4, 413–421, doi:10.5194/acp-4-413-2004, 2004. 253, 266

Seibert, P. and Frank, A.: Source-receptor matrix calculation with a Lagrangian particle dispersion model in backward mode, Atmos. Chem. Phys., 4, 51–63, doi:10.5194/acp-4-51-2004, 2004. 252

Tarantola, A.: Inverse Problem Theory: Methods for Data Fitting and Model Parameter Estimation, Elsevier, Amsterdam, 1987. 251

Uliasz, M.: Lagrangian particle modeling in mesoscale applications, in: Environmental Modelling II, 71–102, Computational Mechanics Publications, 1994. 251

WMO: The Global Atmosphere Watch Programme: 25 Years of Global Coordinated Atmospheric Composition Observations and Analyses, Tech. Rep. WMO-No. 1143, World Meteorological Organization, Geneva, Switzerland, 2014. 249

Ziehn, T., Scholze, M., and Knorr, W.: Development of an ensemble-adjoint optimization approach to derive uncertainties in net carbon fluxes, Geosci. Model Dev., 4, 1011–1018, doi:10.5194/gmd-4-1011-2011, 2011. 249

Ziehn, T., Nickless, A., Rayner, P. J., Law, R. M., Roff, G., and Fraser, P.: Greenhouse gas network design using backward Lagrangian particle dispersion modelling – Part 1: Methodology and Australian test case, Atmos. Chem. Phys., 14, 9363–9378, doi:10.5194/acp-14-9363-2014, 2014. 248, 250, 251, 252, 253, 254, 261

Table 1. Location of existing greenhouse gas measurement stations in Australia. Stations that are currently operational and have been selected for the base network are highlighted in bold typeface. The factor a_{obs} is used to scale the observational uncertainties for CO_2, CH_4 and N_2O in a sensitivity experiment. For Cape Grim and Gunn Point a_{obs} is used in all experiments.

No.	Station	Location lat, lon	Operation period	Measurements in situ	a_{obs}
1	Arcturus	−23.86, 148.47	2010–2014	CO_2, CH_4	2, 1, 1
2	Aspendale	−38.01, 145.01	2003–present	CO_2, CH_4	2, 2, 2
3	Cape Ferguson	−19.30, 147.10	1991–present	–	2, 1, 1
4	**Cape Grim**	−40.70, 144.70	1976–present	CO_2, CH_4, N_2O	0.5, 0.5, 0.5
5	Darwin	−12.42, 130.89	2005–present	CO_2, CH_4, N_2O	1, 1, 1
6	**Gunn Point**	−12.20, 131.00	2011–present	CO_2, CH_4, N_2O	0.75, 0.75, 0.75
7	Otway	−38.31, 142.49	2005–2012	CO_2, CH_4	1, 1, 1
8	Tumbarumba	−35.39, 148.09	2004–2008	CO_2	2, 1, 1
9	Wollongong	−34.41, 150.88	2008–present	CO_2, CH_4, N_2O	1, 1, 1

GID
5, 247–283, 2015

Table 2. Location of potential greenhouse gas measurement stations using the location of the Bureau of Meteorology weather watch radar stations including one additional station at Lucinda Jetty. The factor a_{obs} is used to scale the observational uncertainties for CO_2, CH_4 and N_2O in a sensitivity experiment.

No.	Station	Location lat, lon	a_{obs}	No.	Station	Location lat, lon	a_{obs}
10	Adelaide Airport	−34.95, 138.53	2,1,1	40	Lemon Tree Pass	−32.73, 152.03	2,1,1
11	Albany	−34.95, 117.80	1,1,1	41	Letterbox	−34.26, 150.87	1,1,1
12	Alice Springs	−23.82, 133.90	1,1,1	42	Longreach	−23.43, 144.29	2,1,1
13	Berrimah	−12.46, 130.93	1,1,1	43	Mackay	−21.12, 149.22	2,1,1
14	Bowen	−19.87, 148.08	2,1,1	44	Marburg	−27.61, 152.54	1,2,1
15	Brisbane Airport	−27.39, 153.13	1,2,1	45	Melbourne Laverton	−37.85, 144.75	2,2,2
16	Broeadmeadows	−37.69, 144.95	2,2,2	46	Mildura	−34.23, 142.08	1,1,1
17	Broome	−17.95, 122.23	1,1,1	47	Moree	−29.50, 149.85	2,1,1
18	Buckland Park	−34.62, 138.57	2,1,1	48	Mornington Island	−16.67, 139.17	1,1,1
19	Cairns Airport	−16.88, 145.75	1,1,1	49	Mt Gambier	−37.75, 140.78	1,1,1
20	Cape Range	−22.10, 114.00	1,1,1	50	Mt Kanighan	−25.97, 152.58	1,1,1
21	Captains Flat	−35.66, 149.51	1,2,2	51	Mt Stuart	−19.35, 146.78	1,1,1
22	Canarvon	−24.88, 113.67	1,1,1	52	Perth	−31.95, 115.84	2,2,1
23	Ceduna	−32.13, 133.70	1,1,1	53	Port Hedland	−20.38, 118.63	1,1,1
24	Charleville	−26.42, 146.27	2,1,1	54	Rockhampton	−23.38, 150.47	2,1,1
25	Coffs Harbour	−30.32, 153.12	1,2,1	55	Saddle Mtn	−16.82, 145.68	1,1,1
26	Dampier	−20.65, 116.69	1,1,1	56	Sellicks Hill	−35.33, 138.50	2,1,1
27	Darwin Airport	−12.42, 130.87	1,1,1	57	Sydney Airport	−33.93, 151.17	2,2,1
28	East Sale	−38.12, 147.13	1,2,1	58	Tennant Creek	−19.63, 134.18	1,1,1
29	Esperance	−33.82, 121.83	1,1,1	59	Tindal	−14.51, 132.45	1,1,1
30	Eucla	−31.68, 128.89	1,1,1	60	Townsville	−19.25, 146.77	2,1,1
31	Geraldton	−28.80, 114.70	1,1,1	61	Wagga	−35.17, 147.47	2,1,1
32	Giles	−25.03, 128.30	1,1,1	62	Weipa	−12.67, 141.92	1,1,1
33	Gladstone	−23.85, 151.27	2,1,1	63	West Takone	−41.18, 145.58	1,1,1
34	Gove	−12.28, 136.82	1,1,1	64	Williamtown	−32.80, 151.83	2,1,1
35	Grafton	−29.62, 152.97	1,2,1	65	Willis Island	−16.30, 149.98	1,1,1
36	Halls Creek	−18.23, 127.66	1,1,1	66	Woomera	−31.16, 136.80	1,1,1
37	Hobart Airport	−42.83, 147.51	1,1,1	67	Wyndham	−15.45, 128.12	1,1,1
38	Kalgoorlie	−30.79, 121.45	1,1,1	68	Yarrawonga	−36.03, 146.03	2,2,1
39	Kurnell	−34.02, 151.23	2,2,1	69	Lucinda Jetty	−18.50, 146.40	1,1,1

GID
5, 247–283, 2015

Table 3. Uncertainty reduction (U_R) for the 2 existing stations in the base network in terms of their ability to reduce the uncertainties on CO_2, CH_4 and N_2O flux estimates. The station number is provided in brackets.

Station (No.)	U_R CO_2	U_R CH_4	U_R N_2O
Cape Grim (4)	7.1 %	8.4 %	10.4 %
Gunn Point (6)	11.3 %	4.1 %	3.9 %
Cape Grim (4) + Gunn Point (6)	17.4 %	12.3 %	13.7 %

GID
5, 247–283, 2015

Table 4. Ranking for new stations added to the base network in terms of their ability to reduce the uncertainties on CO_2, CH_4 and N_2O flux estimates individually and in combination (using GWP weights in cost function). The station number is provided in brackets.

Rank	CO_2 stations	CH_4 stations	N_2O stations	Combined GWP
1	Charleville (24)	Tumbarumba (8)	Moree (47)	Charleville (24)
2	Moree (47)	Moree (47)	Longreach (42)	Moree (47)
3	Mornington Island (48)	Perth (52)	Captains Flat (21)	Mornington Island (48)
4	Tumbarumba (8)	Longreach (42)	Perth (52)	Tumbarumba (8)
5	Wyndham (67)	Wyndham (67)	Broadmeadows (16)	Wyndham (67)

GID
5, 247–283, 2015

Table 5. Ranking for new stations added to the base network in terms of their ability to reduce the uncertainties on CO_2, CH_4 and N_2O flux estimates for some of the sensitivity tests: SE1 – using equal contributions of the 3 GHG, SE4 – using GWP weights and distance measure and SE5 – using GWP weights, distance measure and increased observational uncertainties for stations close to large sources. The station number is provided in brackets.

Rank	Combined SE1	Combined SE4	Combined SE5
1	Moree (47)	Moree (47)	Letterbox (41)
2	Longreach (42)	Longreach (42)	Longreach (42)
3	Tumbarumba (8)	Tumbarumba (8)	Moree (47)
4	Perth (52)	Broadmeadows (16)	Captains Flat (21)
5	Mornington Island (48)	Williamtown (64)	East Sale (28)

GID
5, 247–283, 2015
Greenhouse gas network design
T. Ziehn et al.

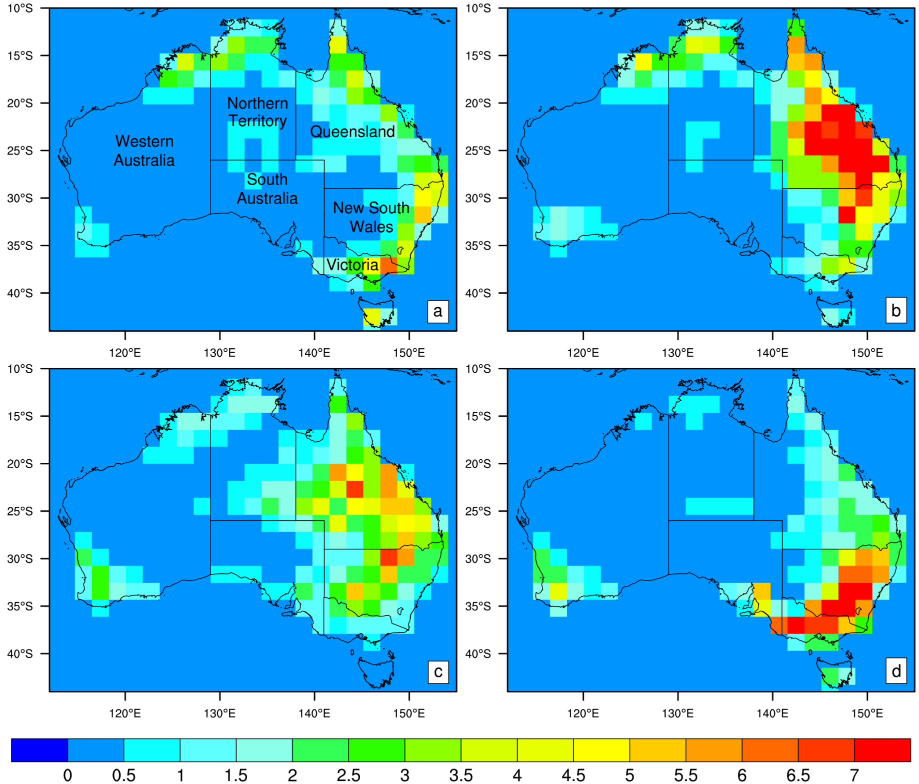

Figure 1. Prior biosphere CO_2 flux uncertainties (1 standard deviation) in grams carbon per square metre per week at 1.8° resolution for the first week in **(a)** January, **(b)** April, **(c)** July and **(d)** October.

GID
5, 247–283, 2015

Greenhouse gas network design

T. Ziehn et al.

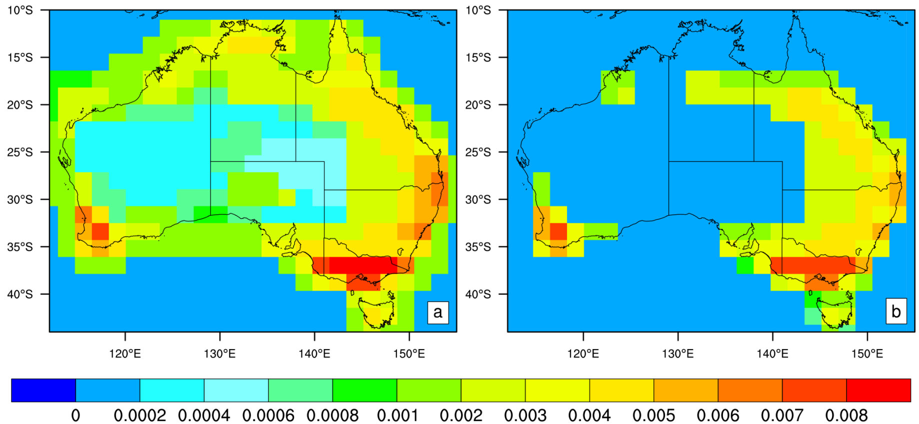

Figure 2. Prior CH_4 flux uncertainties (1 standard deviation) in grams carbon per square metre per week at 1.8° resolution for **(a)** the total and **(b)** ruminant land animals only. The seasonality of the wetland fluxes is not shown here in the total.

GID
5, 247–283, 2015
Greenhouse gas network design
T. Ziehn et al.

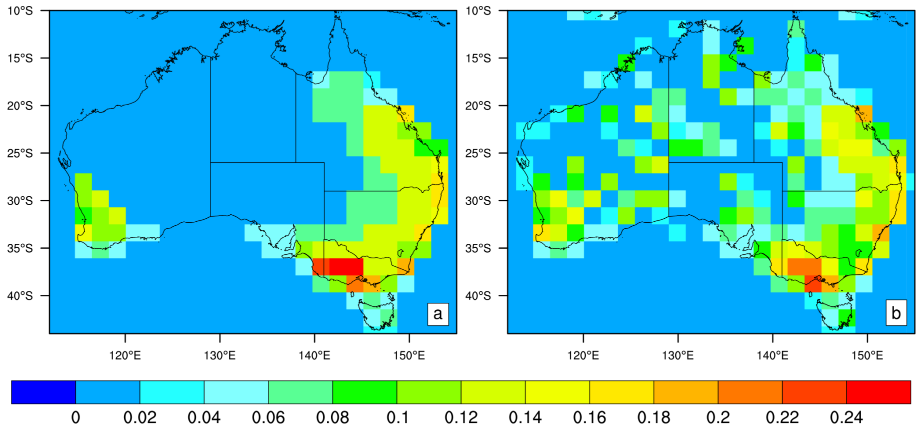

Figure 3. Prior N_2O flux uncertainties (1 standard deviation) in milligrams nitrogen per square metre per week at 1.8° resolution for **(a)** the total (agriculture). The random variation in flux uncertainties used for the sensitivity test is shown in **(b)**.

GID
5, 247–283, 2015

Greenhouse gas network design

T. Ziehn et al.

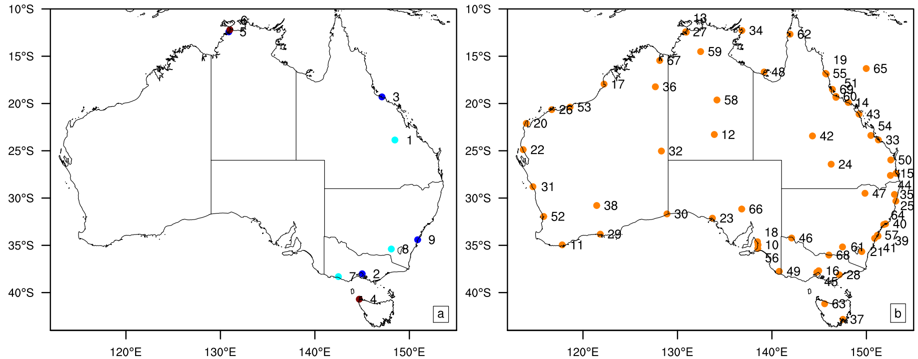

Figure 4. Location of the existing GHG measurement stations in Australia **(a)** and potential sites using mainly the location of the stations in the Bureau of Meteorology's National Radar Loop **(b)**. Station names are provided in Table 1 for existing sites and Table 2 for potential sites. In **(a)** existing stations that are included in the base network are marked in brown and stations that are no longer operational are marked in light blue.

GID
5, 247–283, 2015

Greenhouse gas network design

T. Ziehn et al.

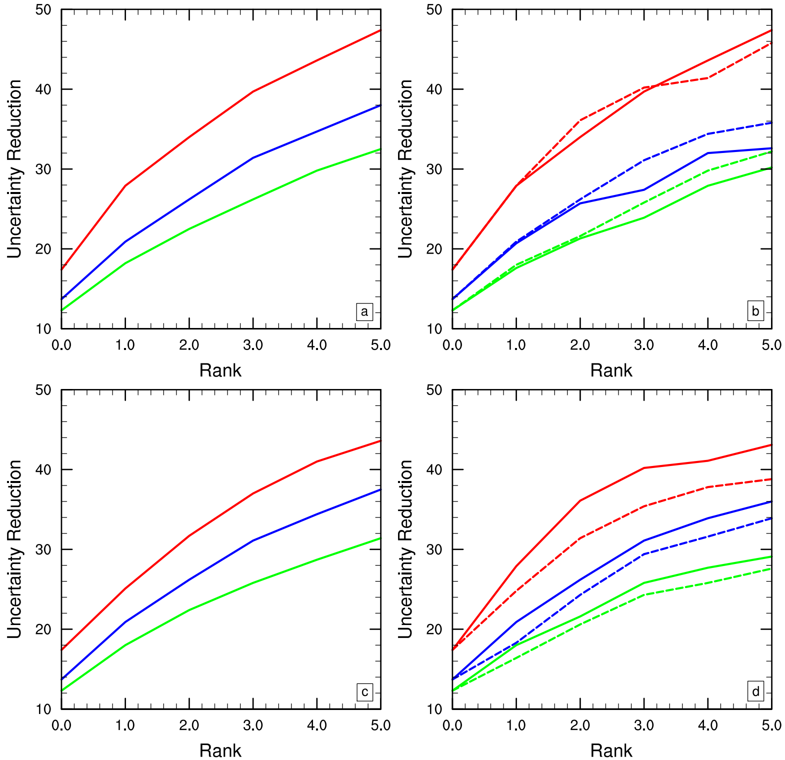

Figure 5. Uncertainty reduction for the 5 stations added to the base network for **(a)** each GHG individually, **(b)** the multi-objective optimization (solid lines: GWP weights, dashed lines: equal weights (SE1)), **(c)** the sensitivity test (SE2) with changed observational uncertainties for each GHG individually, and **(d)** the sensitivity test (SE4) with multi-objective optimization using GWP weights that also includes the distance (solid lines) and SE5 (dashed lines) (red: CO_2, green: CH_4 and blue: N_2O).

GID
5, 247–283, 2015

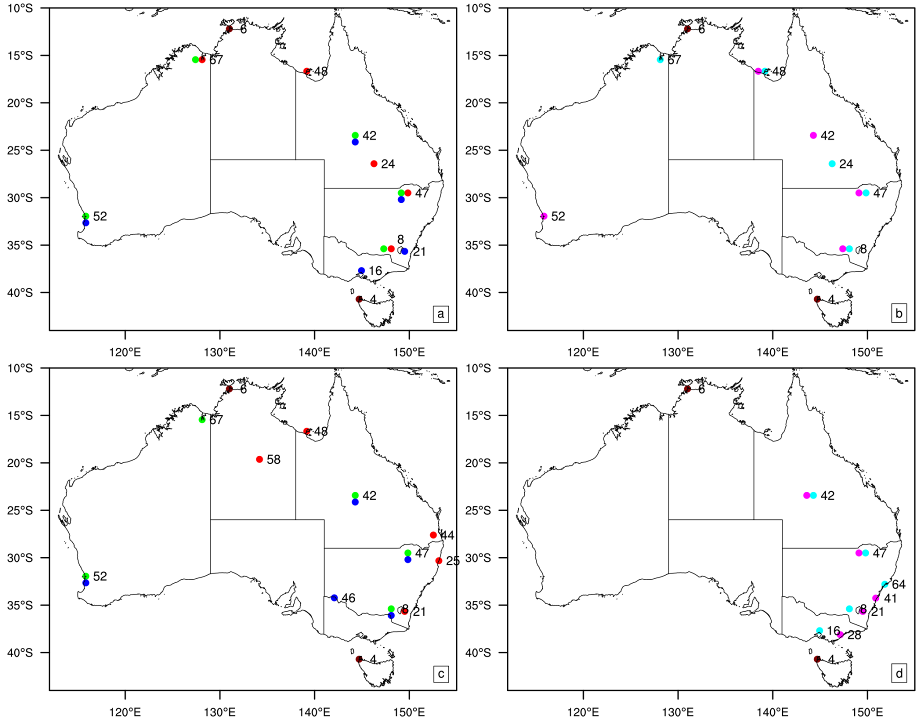

Figure 6. Location of the proposed GHG measurement stations in Australia using the network design for **(a)** each GHG individually (red: CO_2, green: CH_4 and blue: N_2O), **(b)** the multi-objective optimization (light blue: GWP weights, pink: equal weights – SE1), **(c)** the sensitivity test (SE2) with changed observational uncertainties for each GHG individually (red: CO_2, green: CH_4 and blue: N_2O) and **(d)** the sensitivity test (SE4) with multi-objective optimization using GWP weights that also includes the distance (light blue) and SE5 (pink). The location of the stations in the base network are marked in brown.

GID
5, 247–283, 2015

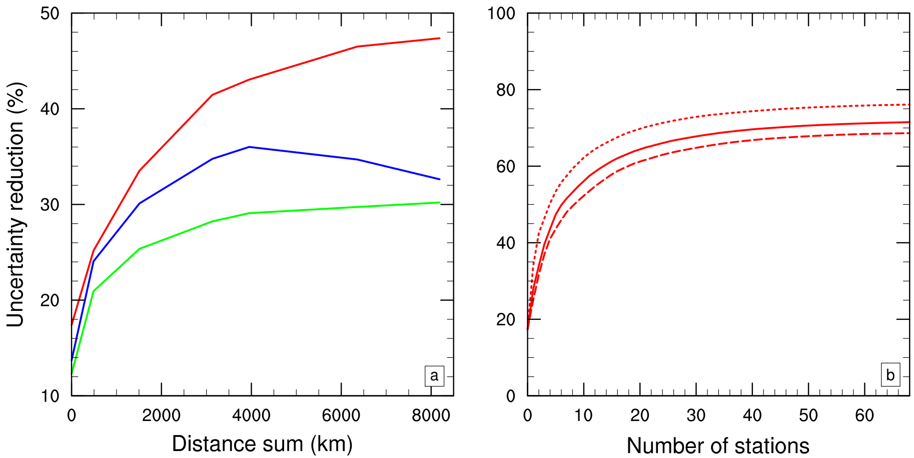

Figure 7. (a) Uncertainty reduction for the 3 GHGs (red: CO_2, green: CH_4 and blue: N_2O) with respect to the total distance to Aspendale for the 5 stations in the network extension and **(b)** uncertainty reduction for CO_2 for the default case (solid line), increased observational uncertainties SE2 (dashed line) and observational uncertainty for all stations set to almost zero (dotted line).

GID
5, 247–283, 2015
Greenhouse gas network design
T. Ziehn et al.